Water Air Soil Pollut (2018) 229: 357
https://doi.org/10.1007/s11270-018-3988-6

Effect of Humic Acid on the Nitrate Removal by Strong Base Anion Exchanger Supported Nanoscale Zero-valent Iron Composite

Luyao Wang · Hongguang Zhou · Jie Liu · Jie Chen · Shiqiang Wei · Zhenmao Jiang

Received: 10 July 2018 / Accepted: 18 September 2018 / Published online: 25 October 2018

Abstract To probe the effect of common coexist substances on the nitrate removal by polymeric resin supported nanoscale zero-valent iron composite (D201-nZVI), humic acid (HA) was added into the nitrate removal system to elaborate the different interactions between each two and among all in the system including HA, nitrate, and D201-nZVI. The results showed that the effect of HA on the reduction of nitrate by D201-nZVI was concentration-dependent. At low HA concentration (< 5 mg/L), HA coating formed by the HA adsorption on the surface of the nZVI particles enhanced the dispersion of the particles, which led to a more evenly distribution of nZVI particles in the solution, and thus a higher nitrate reduction activity. When HA concentration was increased to 5 mg/L or more, the competitive adsorption of HA and NO_3^- on the surfaces of the D201-nZVI dominated, and the nitrate removal rate and ammonia nitrogen production were decreased. When the HA concentration reached to a further high level (> 20 mg/L), HA acted as an electron shuttle to accelerate the reduction of Fe(III) to Fe(II) in the D201-nZVI, and thus the nitrate reduction rate was accordingly enhanced. The ammonia production increased by 24.8% at HA concentration of 40 mg/L as compared with that of the control (without addition of HA). This research elucidated the interaction of HA within different HA concentration in the complicate system of anions removal by organic support-nanoscale metal particle composite, which may shade some new light on the potential application of nanoscale zero-valent materials in the practical remediation of natural water.

Keywords Nanoscale ZVI · Humic acid · Polymeric resins · Nitrate removal · Complexation

Electronic supplementary material The online version of this article (https://doi.org/10.1007/s11270-018-3988-6) contains supplementary material, which is available to authorized users.

L. Wang · H. Zhou · J. Liu · J. Chen · S. Wei · Z. Jiang (✉)
The Key Laboratory of Agricultural Resources and Environment in Chongqing, College of Resource and Environment, Southwest University, Chongqing 400716, People's Republic of China
e-mail: windring@swu.edu.cn

L. Wang
Institute of Land Engineering and Technology, Shaanxi Provincial Land Engineering Construction Group Co., Ltd., Xi'an 710075, China

1 Introduction

Since the 1990s, nanoscale zero-valent iron (nZVI) has been widely applied in water/soil remediation (Li et al. 2006; Crane and Scott 2012) due to its outstanding characteristic such as large specific surface area and strong reducing activity. The nZVI materials were applied in the reduction of NO_3^- (Hwang et al. 2011; Jiang et al. 2011; Ryu et al. 2011), Cr(IV) (Lv et al. 2012; Zhang et al. 2018), Pb(II) (Kim et al. 2013; Shi et al. 2013), and As (Klas and Kirk 2013; Neumann et al. 2013) and dehalogenation of organic contaminants such as chloroethenes (Liu et al. 2005a), trichloroethene (Liu et al. 2005b), azo-dyes (Luo et al. 2013), phenol

(Shimizu et al. 2012), polycyclic aromatic hydrocarbons (PAHs) (Chang et al. 2005), herbicides (Joo et al. 2004), etc. The increasing discharges of nitrate from various sources, such as agricultural fertilizers, septic-tank systems, animal wastes, industrial processes, and atmospheric deposition, led to high nitrate concentration in the surface water and groundwater (Xu et al. 2012; Song et al. 2013). Excessive nitrate concentrations in drinking water sources may bring some potential risks to the environment and public health, including methemoglobinemia, liver damage, and even cancer (Bhatnagar and Sillanpää 2011). Many technologies have been developed to remove nitrate effectively, such as adsorption, ion exchange, electrodialysis, reverse osmosis, chemical treatment (Song et al. 2013), etc.

In recent decades, the application of nZVI to remove nitrate from water has been intensively addressed. The factors controlling nitrate removal efficiency by nZVI were the main focuses, such as the dosage of nZVI, experimental conditions (temperature and pH) (Liao Dijie 2009; Song et al. 2013), size of ZVI particles, passivation process of nZVI (Sohn et al. 2006), addition of inorganic and organic matters (Cl^-, SO_4^{2-} (Su and Puls 2004, Zhang et al. 2013a, 2013b, Zhang et al. 2017), propanol (Liao et al. 2003), etc.). It is worth noting that the geochemical characteristics of water solution (e.g., ionic strength, humic substances (HS)) (Manciulea et al. 2009) play an important role in the stability of nZVI, which would determine its chemical activity to a great extent. Particularly, as the most widely existed natural organic matter (NOM) on the earth, humic acids (HAs) play important roles both in controlling the environmental behaviors of pollutants (Buffle 2006; Chen et al. 2011) and in affecting the water treatment efficiency due to their abundant functional groups and high reactivity. Recent reports have shown that NOM can stabilize suspensions of iron oxide nanoparticles by changing the surface charges, then influencing its aggregation and sticking, which is related to solution pH and the concentration of HA (Baalousha 2009, Yang et al. 2009), and therefore affects its in situ mobility. Richard et al. proved that the mobility of nZVI through granular media is greatly increased when NOM (Johnson et al. 2009) was added. Complexation between HA and iron oxides may alter the properties of the composite and thus its ability to reduce nitrate, which is also pH-dependent. Seunghun Kang et al. (Kang and Xing 2008) demonstrated that goethite had a strong adsorption on HA, and the adsorption rate decreased with the increase of pH values due to the changes of electrostatic interaction and complexation between the acidic functional group of HA and the surface of the goethite. However, there is no report currently available concerning the effect of HA on the reduction capacity of nitrate by nZVI, nor does the polymeric resin supported nanocomposites.

In our previous research (Jiang et al. 2011), polymerstyrene anion exchange resin was adopted to be the organic support of nZVI. The internal network structure of polymeric resin provided sufficient sites for the immobilized nZVI particles; and its inherent charged functional groups can make nZVI particles disperse evenly and keep them in smaller size and a higher activity (Zhang et al. 2013a, 2013b). When HA emerged as a coexisting matter with nitrate in the removal system by this composite, HA may influence the electrostatic attraction of the nitrate and quaternary ammonium group of the resins, and meanwhile the reduction of nitrate by nZVI. Consequently, the main objective of the current study is to elucidate the effects and mechanism of HA on the support resin and nZVI in the complicated system. Firstly, we compared the HA adsorption behaviors on polymer and D201-nZVI with and without nitrate, respectively, to explain the exact interaction between HA and polymer/nZVI. Afterward, some structural characterizations during these interactions were offered to demonstrate these interactions and the structure changes of nZVI. The results of this study may shade new light on the potential application of nZVI composite in the practical remediation of natural water.

2 Materials and Methods

2.1 Materials

All chemicals used in this study were of analytical reagent grade. The support material D201 macroporous anionic exchanger, a polystyrene-divinylbenzene polymer matrix with tetra amine as functional groups, was purchased from Zhejiang Zhengguang Industrial Co., Ltd., China. Prior to use, it was rinsed in turn with NaOH (5 wt%), HCl (5 wt%), and finally distilled water to a neutral pH, and dried at 40 °C for 24 h. All solutions were prepared by ultrapure water with resistivity of 18.25 MΩ. Humic acid was bought from Tianjin Guangfu Technology Development Co., Ltd. which

was extracted from weathered coal. HA sample was firstly dissolved by ultrapure water, then adjusted the solution pH to about 10 with 0.1 M NaOH. Afterward, HA solution was ultrasonic shocked for 2 h to let it fully dissolve, then adjust the pH to 7 with 0.1 M HCl. At last, HA solution was filtered through 0.45-μm membranes after being shocked for 24 h at room temperature. All prepared solutions were stored at 4 °C in the dark for use.

2.2 Preparation of D201-nZVIs

The ultrapure water with resistivity of 18.25 MΩ was kept at room temperature under N_2 gas purging for at least 1 h, then it was used for preparation of nZVI to avoid its oxidation during the modification process. Preparation of the polymer-supported nZVI has been described in detail in our previous study (Jiang et al. 2011). In brief, 1.0 g of dry D201 resin beads were added into 100 mL $FeCl_4^-$ solution that consists of 2.0 M $FeCl_3$, 2.0 M HCl, and 10% ethanol. As the precursor of nZVI, the anionic $FeCl_4^-$ was ion-exchanged with the counter Cl^- ions of D201. After 12 h rotation in an end-over-end shaker, the solid beads were obtained by filtration and rinsed five times with ethanol, and then introduced into $NaBH_4$ solutions with mass concentrations of 3%. After 15 min, the preloaded $FeCl_4^-$ ions could be reduced into ZVI. The composites were freshly prepared before each experiment, and the materials used for structural characterization were dried in a vacuum oven at 40 °C for 24 h.

2.3 HA Adsorption

Each of 0.1 g D201 or the new synthesized D201-nZVI with the same amount of D201 was added into 50 mL mixed solution of different concentrations (0, 1.0, 2.0, 5.0, 7.5, 10, 15, 20, 30, 40 mg/L) of HA and 50 mg/L NO_3^--N, respectively. Then shaken at a constant temperature of 298 K for 12 h at 120 rpm in a thermostatic water bath shaking bed. The HA contents in the solutions before and after the reaction were measured.

2.4 Nitrate Reduction

In all batch experiments, the dosages of the resin (D201) were set as 2.0 g/L. To investigate the performance of nitrate removal by nanocomposites, its beads were introduced into 50 mL solution containing 50 mg N/L nitrate and different concentration (0, 1.0, 2.0, 5.0, 7.5, 10, 15, 20, 30, 40 mg/L) of HA. The suspension was stirred for 8 h at 120 rpm at constant temperature of 298 K and initial pH 7.0 ± 0.1, then followed by filtering through 0.45-μm membranes. Afterward, 10 mL HCl was added to dissolve the precipitate on the membranes to determine its Fe amount. At last, 2.0 mL solution after nitrate reduction was sampled for analyzing the remaining concentration of nitrate, nitrite, and ammonium, respectively.

Kinetic tests were carried out to establish the effect of contact time on the reduction process and to quantify the reduction rate. Two grams of D201 after loaded on nZVI was added to a flask containing 1000 mL solution mixed together with 50 mg/L NO_3^--N and different concentration of HA (1, 5, 15, 40 mg/L) at 298 K with the stirring rate at 120 rpm. Meanwhile, NO_3^--N removal by composites in the absence of HA was conducted as a control. Then, the concentration of residual nitrate, nitrite, and ammonium in the solution was determined at regular time intervals by the methods described in the following section.

2.5 Characterization

Fourier transform infrared (FT-IR) spectra of D201 resin and D201-nZVI before and after adsorption or reduction were recorded at room temperature on a Spectrum GX spectrophotometer (Nicolet IS10). The morphology and interaction of nitrate and HA on the inner surface of nanocomposites were probed by a transmission electron microscope (TEM, JEM 1200EX, Japan) and X-ray photoelectron spectrometer (XPS, ESCALAB-2, UK) equipped with an Al KD anode as the excitation source. The binding energies were corrected using C1s calibration energy of 285 eV. The XPS results were collected in binding energy forms and fitted using the software of XPSPEAK 41. Transmission electron microscopy (TEM) images and electron diffraction pattern of the nanoparticles were obtained with JEM1200 and GAF20, respectively.

2.6 Analyses

Ammonia concentrations in the solutions were determined by Nessler's reagent colorimetry (Eaton et al. 1995) with a UV-Vis spectrophotometer (Model 722, Shanghai Xianke Spectral instrument Industrial Co., Ltd., China). The resin surface area and pore structure

characterization of D201 and D201-nZVI were determined by N_2 adsorption instrument (Nova 3000 Quantachrome Instruments American). The concentrations of nitrate and nitrite were determined by ion chromatography (DIONEX DX-120) with a column of ionPAC AS14, and the mobile phase was 0.3 M $NaCO_3$/0.1 M $NaHCO_3$ with 1.0 mL/s flow rate. Humic acid was determined spectrophotometrically by measuring the absorbance at $\lambda max = 254$ nm (Horiba JY Aqualog), and the standard curve was made to determine the residual concentration (Fig. S1).

3 Results and Discussion

3.1 HA Adsorption on D201 and D201-nZVI

The electrostatic interaction between HA and D201 and complexation between HA and iron oxides on nZVI may occur in the coexistence system of HA, NO_3^--N, and D201-nZVI, which may affect the nitrate reduction processes. Therefore, we first discuss HA adsorption on D201/D201-nZVI to further explore the mechanism of the HA effect on the nitrate reduction by D201-nZVI.

The adsorption of HA on D201 resin is showed in Fig. 1a. When the initial concentration of HA is in the range of 0~40 mg/L, the adsorption capacities of HA were decreased with the increase of NO_3^--N concentration, which indicated that there was a competitive adsorption between HA and NO_3^- on the single resin system.

Figure 1b shows the adsorption of HA on D201-nZVI. It was shown that HA adsorption was about 2 mg/g at HA concentration of 40 mg/L, even slightly lower than that on the D201 resin (4.3 mg/g). However, the HA adsorptions were dramatically increased when the target pollutant NO_3^--N was added to the D201-nZVI system, which can be caused by both pore size and limited iron oxide content. Data in Table A1 shows that the specific pore size of D201-nZVI was lower than that of the support resin, indicating that nZVI occupied a small amount of active sites on the carrier. Then, HA with larger molecular weight will be blocked when it is entering the resin channel. It has been reported that Fe(0) particles are mainly composed of inner Fe(0) core and outside Fe(II)/Fe(III) oxide shell in water environment (Kumar et al. 2014). XPS analysis of the new synthesized D201-nZVI (Fig. S2) shows that the peak of 707.4 eV and 710.6 eV represented Fe(0) and iron

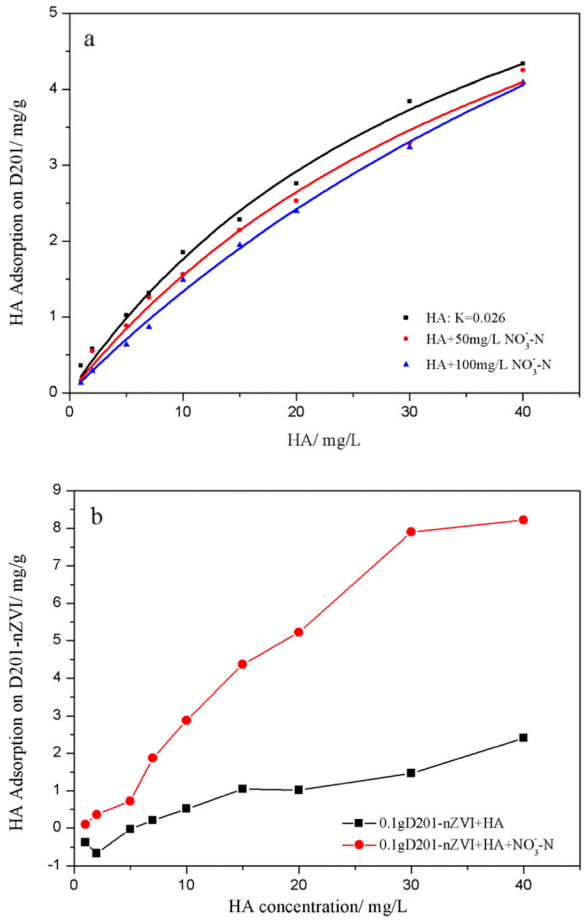

Fig. 1 Adsorption of different concentration of HA on D201 (**a**) and D201-nZVI (**b**)

oxide, respectively, and the surface of D201-nZVI is mostly characterized by the peak of iron oxide peak, and the peak of Fe(0) is weak. After Ar^+ sputtering of D201-nZVI for 1 min, there is a significant Fe(0) signal, accounting for 51.34%, which confirmed that the presence of nZVI surface oxide shell exerts a certain protective effect on the internal Fe(0). The interaction between HA and iron oxides was limited, and related reactions will be described below.

3.2 Effect of pH

In addition to the above two reasons, pH also plays an important role, which will directly influence the type of action between HA and iron oxide. The initial pH of all the reaction systems was 7.2, and as shown in Fig. 2, pH increased to above 8 because of the following reactions (Su and Puls 2004; Li et al. 2006; Calderon and Fullana

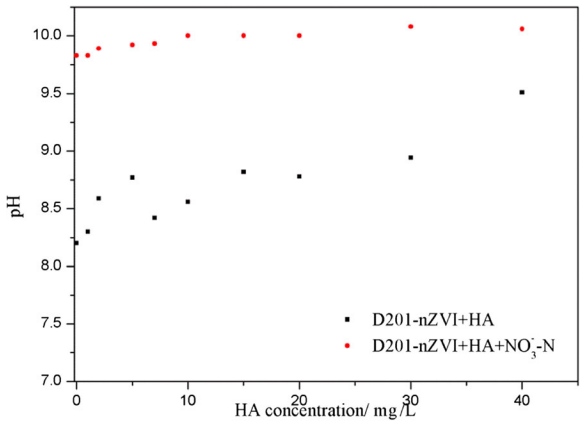

Fig. 2 Solution pH of the two systems under different concentrations of HA

2015):

$$Fe^{0}_{(s)} + 2H_2O_{(aq)} \rightarrow Fe^{2+}_{(aq)} + H_{2(g)} + 2OH^{-}_{(aq)} \quad (1)$$

$$2Fe^{0}_{(s)} + 2H_2O_{(aq)} + O_2 \rightarrow 2Fe^{2+}_{(aq)} + 4OH^{-}_{(aq)} \quad (2)$$

The initial pH (7.2) of the HA and D201-nZVI mixed solution was slightly lower than the isoelectric point of iron oxide (Illés and Tombácz 2006) (pH = 7.9 ± 0.1). The electrostatic attraction existed between iron oxides on the surface of D201-nZVI and HA due to their positive and negative charges at their surfaces at pH 7.2 (Illés and Tombácz 2004), respectively. However, Fe(0) will be impeded to be continuously oxidized due to the protection of nZVI oxides, and with the pH increase, the electrostatic adsorption was very limited.

Meanwhile, it has been found that when the system pH was getting higher, ligand exchange-surface complexation between HA and iron oxides on the surface of nZVI (Vindedahl et al. 2016) would dominate. Tombacz (Tombácz et al. 2013) and Seunghun (Kang and Xing 2008) found that carboxylic acid groups or hydroxyl groups in organic acids and hydroxyl groups on Fe–OH may form iron-carboxylate complexes, and the amount of complex bond is proportional to the content of carboxylic acid, as depicted in the following reaction:

$$Fe{-}OH + R{-}COO^{-} \leftrightarrow Fe{-}OOC{-}R + OH^{-} \quad (3)$$

This was also confirmed by infrared spectroscopy analysis as shown in Fig. 3. The major bands of HA are exhibited as follows: 1049 cm^{-1} (C–O stretching of primary alcohol), 1380.23 cm^{-1}, and 1568.55 cm^{-1} (symmetric stretching of COO–, C–OH stretching of phenolic OH) (Li and Shang 2005). The vibration of C–H (1331.00 cm^{-1}) and the bending vibration of C=C (1586.71 cm^{-1}) in quaternary ammonium of composites were shifted to 1337.96 cm^{-1} and 1584.57 cm^{-1} after HA adsorption, respectively. These findings explained that carboxylic or phenolic functional groups of HA might be attracted through electrostatic by the surface quaternary ammonium groups of composite or be complexed with iron oxides (Kang and Xing 2008). There was a strong peak (1584.63 cm^{-1}, N–H) after nitrate addition into the system that consisted of D201-nZVI and HA, which indicated that nitrate was reduced by nZVI, and the displacement of peaks (C–H, C=C) also proved that there was adsorption or/and complexation between HA and iron oxides.

Therefore, when the target pollutant NO_3^--N was added to the system, iron oxides will be produced continuously due to the reaction between nZVI and NO_3^--N. With the increase of HA concentration, the adsorption of HA on D201 increased, and the complexation reaction with iron oxides was enhanced, which resulted in a significant increase of HA adsorption.

It is commonly known that the size and morphology of nZVI particles will affect its reactivity. It can be observed from the TEM images of the original D201-nZVI and that with HA absorbed (Fig. 4a, b), and nZVI particles were distributed evenly on the original D201-nZVI, which existed as approximately spherical particles with the size of about 20 nm. After the adsorption of HA, the nZVI particles were more evenly distributed on the surface, and the particle size was about 10~15 nm. It can be deduced that the activity of nZVI may be enhanced upon addition of HA at concentration of 20 mg/L.

Besides, it was also found that iron precipitate was formed in the reaction system of nitrate, HA, and D201-nZVI, which was attributed to the following reactions in the alkaline system:

$$Fe^{2+} + OH^{-} \rightarrow Fe(OH)_{2(S)} \quad (4)$$

$$4Fe(OH)_{2(S)} + O_2 + 2H_2O \rightarrow 4Fe(OH)_{3(S)} \quad (5)$$

The iron precipitate produced was HA-concentration relevant. When the addition of HA was

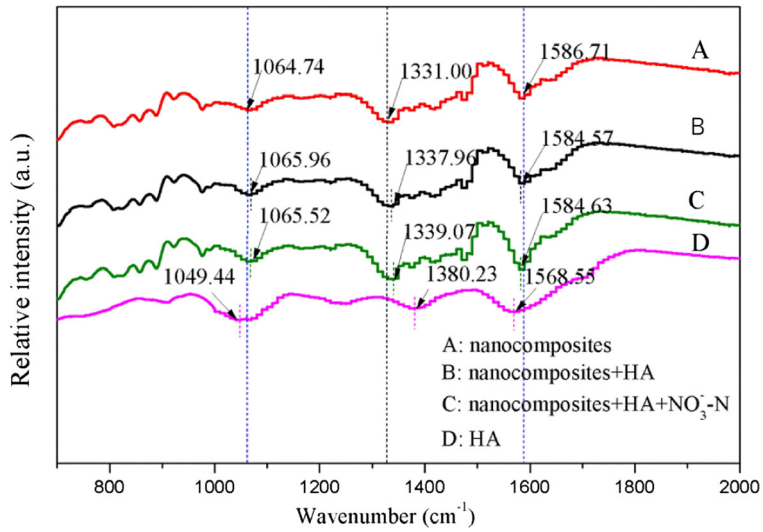

Fig. 3 FT-IR spectra of D201-nZVI before and after it reacted with HA or/and NO_3^--N

lower than 20 mg/L, the electrostatic interaction between HA and iron oxides on the surface of nZVI dominated, causing evenly HA coating on the nZVI particles, and thus impeding the iron precipitation (as shown in Fig. S3). The similar phenomena were also found for nano-metal oxide such as nano-TiO_2 (Zhang et al. 2008) and silver nanoparticles (Delay et al. 2011). With the increase of HA concentration, the complexation between HA and iron oxides was enhanced, and the solution pH was increased (as shown in Fig. 2) and accordingly more iron precipitation was also formed (as shown in Fig. S3). The addition of the target contaminant NO_3^--N in the system resulted in a significant increase in pH and iron precipitation (as shown in Fig. 2 and Fig. S3).

3.3 Effect of HA on the Reduction of Nitrate by D201-nZVI

Following the discussion of the interaction between HA and D201-nZVI in the experimental system, we focused on the static removal of NO_3^--N by D201-nZVI at different HA concentrations. The possible pathways for nitrate removal in the reaction system included both adsorption by support carrier D201 resin through electrostatic attraction and reduction reaction by nZVI. The production of ammonia, the main reduction products of nitrate, is often used to evaluate the reduction activity of nZVI. The overall reaction of nitrate reduction by nZVI can be represented as follows (Su and Puls 2004; Sohn et al. 2006):

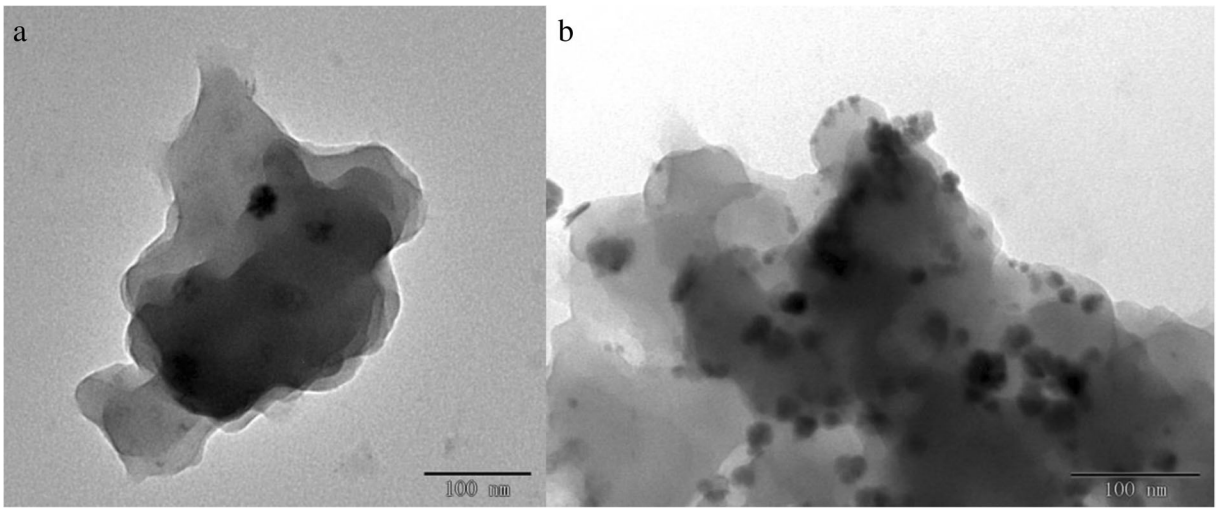

Fig. 4 TEM images of **a** D201-nZVI and **b** D201-nZVI with HA absorbed at HA concentration of 20 mg/L

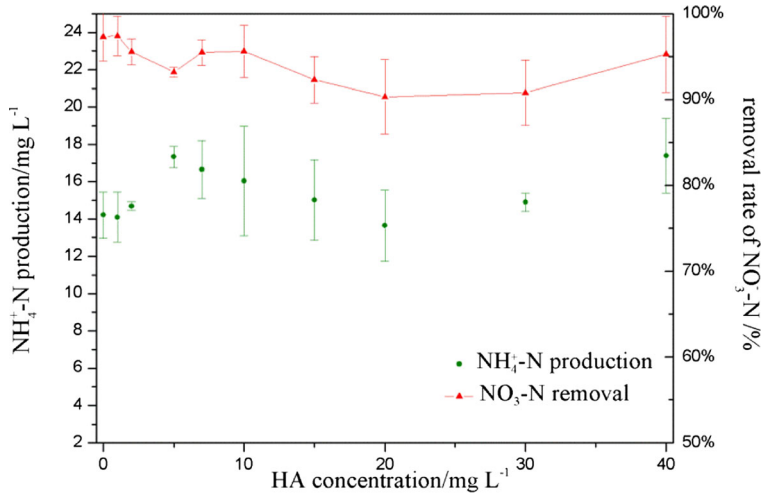

Fig. 5 Ammonia production and removal rate of nitrate at different concentration of HA (initial nitrite, 50 mg/L; T, 298 K; initial pH, 7; ZVI for all the reaction mixtures was the same and equal to 13.2~14.3Fe% in mass)

$$NO_3^- + 4Fe^0 + 10H^+ \leftrightarrow NH_4^+ + 4Fe^{2+} + 3H_2O \quad (6)$$

In the neutral system of this article, we changed the equation to the following:

$$NO_3^- + 4Fe^0 + 7H_2O \leftrightarrow NH_4^+ + 4Fe^{2+} + 10OH^- \quad (7)$$

Figure 5 combines the ammonia production and nitrate removal rate at HA concentration of 0–40 mg/L, from which the reduction activity of nitrate by nZVI as influenced by HA can be analyzed. It can be seen that the average yield of ammonia was 14.21 mg/L in the absence of HA, and the removal rate of nitrate in the solution was 97.3%. When 5 mg/L of HA was added, the production of ammonia was increased to 17.33 mg/L,

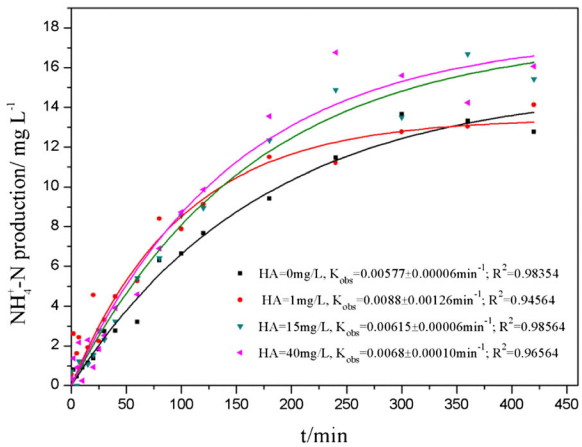

Fig. 6 Nitrite reduction kinetics by D201-nZVI at different concentration of HA: 0 mg/L, 1 mg/L, 15 mg/L, 40 mg/L (initial nitrite, 3.57 mM; T, 298 K; initial pH, 7; ZVI for all the reaction mixtures was the same and equal to 13.2~14.3Fe% in mass)

which is due to the well dispersion of the nZVI particles, and thus the better performance in the reduction of nitrate. When the HA concentration was increased to 20 mg/L, the competitive adsorption of HA and NO_3^--N on D201-nZVI gradually dominated, which resulted in a decreased removal rate of NO_3^--N and ammonia production. With the further increase of HA concentration (20–40 mg/L), the complexation between HA and iron oxides on the surface of nZVI enhanced. Through the electron diffraction analysis of D201-nZVI after adsorbed HA (without nitrate), it is found that there was Fe_3O_4 on the surface of the particles (Fig. S4), it could be inferred that Fe(III) was reduced to Fe(II) by HA, thus improving the NO_3^--N reduction ability of D201-nZVI, which was also confirmed by XPS analysis. When the concentration of HA is 0, 2, and 40 mg/L, the Fe(II) contents of nanocomposites were 6.84%, 4.40%, and 4.57%, respectively (Fig. S5). The above findings may be due to the participation of Fe^{2+} in the redox reaction after HA added. And it is worth noticing that other scholars have come to the same conclusion. Li Xie (2005) pointed out that the redox-active functional groups in humic acid can reduce Fe(III) to Fe(II), and the oxidized functional groups in the humic acid may also be reduced by Fe(0), then electrons are given to the electron acceptor to improve the removal of contaminants rate. Jiang Xu (Xu et al. 2012) proved that NO_3^--N reduction by Fe(0) on the metal surface usually depends on the electron transfer efficiency of the oxide surface from Fe(0) to the active site, and the addition of a certain amount of Fe^{2+} to the reaction system can increase the removal rate of NO_3^--N.

3.4 Effect of HA on the Nitrate Removal Kinetics

The effect of HA on the kinetics of nitrate reduction by D201-nZVI is another important aspect concerning its application for environmental remediation. As shown in Fig. 6, the ammonia production kinetics at different HA concentration were well fitted by traditional pseudo-first-order kinetic model expressed as follows:

$$\frac{d[C]_t}{dt} = k_{obs}\left([C]_e - [C]_t\right) \quad (8)$$

where k_{obs} (min^{-1}) and $[C]_t$ represent the pseudo-first-order rate constant and the ammonium concentration at time t, respectively. The following equation can be obtained by integrating

$$[C]_t = [C]_e\left(1 - e^{-k_{obs}t}\right) \quad (9)$$

Figure 6 shows that the k_{obs} of NH_4^+-N production was 0.00577, 0.0088, 0.00615, and 0.0068 min^{-1} when the HA concentration was 0, 1, 15, and 40 mg/L respectively. The adsorption kinetics usually depend on three main steps, namely, external diffusion, intra-particle diffusion, and the interaction between the adsorbate and the adsorbent (Shuang et al. 2013). Since the concentration of target pollutant NO_3^--N is fixed, its external diffusion rate remains unchanged, basically. When HA concentration was 1 mg/L, nZVI particles were distributed more evenly, and the internal diffusion rate of NO_3^--N also increased. Therefore, the reaction rate increased. Due to the competitive adsorption between HA and NO_3^--N, the interaction between D201-nZVI and NO_3^--N decreased after HA addition, which reflected a slight decrease in the reaction rate at HA concentration of 15 mg/L. When HA concentration was increased to 40 mg/L, the above two factors balanced, and the electron transfer of HA could promote the reaction rate.

When the reaction reached equilibrium, the concentration of ammonia nitrogen is consistent with the result of 3.2 following the similar reasons described thereby.

4 Conclusions

The present study demonstrated that the concentration of HA brought various influences to the capacity of D201-nZVI. In general, the results suggest three mechanisms: (1) the competitive adsorption between HA and NO_3^--N on D201 resin; (2) the electrostatic of HA and iron oxide on nZVI surface below the iron oxide isoelectric point and the complexation of both two at high pH; (3) the electron transfer of HA. The predominant mechanism for nitrate reduction by D201-nZVI varies with the HA concentrations.

When the HA concentration is low (< 5 mg/L), HA coating formed due to a small amount of HA adsorbed on the surface of nZVI particles caused a well dispersion of nZVI particles in the solution, thereby enhancing its nitrate reduction performance. When the concentration of HA increased to 5 mg/L or more, the competitive adsorption of HA and NO_3^--N was dominant, and the removal rate of NO_3^--N and ammonia production decreased. When HA is further improved to more than 20 mg/L, Fe(III) is reduced to Fe(II) by the electron transfer of HA, and the reduction of NO_3^--N is improved. The results show that it is necessary to consider the presence of HA in waters when using nanocomposites to remove nitrate, and the behavior of nanocomposites in natural systems needs more attention. Further studies should be extended to a wider and more representative range of conditions, such as HA of different origins or molecular weight and other constituents in groundwater.

Acknowledgments This research is supported by the Natural Scientific Foundation of China (Grant No. 21207110 and 41771347) and the National Key Research and Development Program of China (2017YFD0800903).

References

Baalousha, M. (2009). Aggregation and disaggregation of iron oxide nanoparticles: influence of particle concentration, pH and natural organic matter. *The Science of the Total Environment, 407*(6), 2093–2101.

Bhatnagar, A., & Sillanpää, M. (2011). A review of emerging adsorbents for nitrate removal from water. *Chemical Engineering Journal, 168*(2), 493–504.

Buffle, J. (2006). The key role of environmental colloids/nanoparticles for the sustainability of life. *Environment and Chemistry, 3*(3), 155–158.

Calderon, B., & Fullana, A. (2015). Heavy metal release due to aging effect during zero valent iron nanoparticles remediation. *Water Research, 83*, 1–9.

Chang, M. C., Shu, H. Y., Hsieh, W. P., & Wang, M. C. (2005). Using nanoscale zero-valent iron for the remediation of polycyclic aromatic hydrocarbons contaminated soil. *Journal of*

the Air & Waste Management Association, 55(8), 1200–1207.

Chen, J., Xiu, Z., Lowry, G. V., & Alvarez, P. J. (2011). Effect of natural organic matter on toxicity and reactivity of nano-scale zero-valent iron. *Water Research, 45*(5), 1995–2001.

Crane, R. A., & Scott, T. B. (2012). Nanoscale zero-valent iron: future prospects for an emerging water treatment technology. *Journal of Hazardous Materials, 211-212*, 112–125.

Delay, M., Dolt, T., Woellhaf, A., Sembritzki, R., & Frimmel, F. H. (2011). Interactions and stability of silver nanoparticles in the aqueous phase: influence of natural organic matter (NOM) and ionic strength. *Journal of Chromatography. A, 1218*(27), 4206–4212.

Eaton, A. D., Clescerl, L. S., & Greenberg, A. E. (1995). *Standard method for the examination of water and waste water* (19th ed.). Washington, DC: American Public Health Association, American Water Works Association, Water Environment Federation.

Hwang, Y. H., Kim, D. G., & Shin, H. S. (2011). Mechanism study of nitrate reduction by nano zero valent iron. *Journal of Hazardous Materials, 185*(2–3), 1513–1521.

Illés, E., & Tombácz, E. (2004). The role of variable surface charge and surface complexation in the adsorption of humic acid on magnetite. *Colloid Surface A, 230*(1–3), 99–109.

Illés, E., & Tombácz, E. (2006). The effect of humic acid adsorption on pH-dependent surface charging and aggregation of magnetite nanoparticles. *Journal of Colloid and Interface Science, 295*(1), 115–123.

Jiang, Z., Lv, L., Zhang, W., Du, Q., Pan, B., Yang, L., & Zhang, Q. (2011). Nitrate reduction using nanosized zero-valent iron supported by polystyrene resins: role of surface functional groups. *Water Research, 45*(6), 2191–2198.

Johnson, R. L., Johnson, G. O., Nurmi, J. T., & Tratnyek, P. G. (2009). Natural organic matter enhanced mobility of nano zerovalent iron. *Environmental Science & Technology, 43*, 5455–5460.

Joo, S. H., Feitz, A. J., & Waite, T. D. (2004). Oxidative degradation of the carbothioate herbicide, molinate, using nanoscale zero-valent iron. *Environmental Science and Technology, 38*, 2242–2247.

Kang, S., & Xing, B. (2008). Humic acid fractionation upon sequential adsorption onto goethite. *Langmuir, 24*, 2525–2531.

Kim, S. A., Kamala-Kannan, S., Lee, K. J., Park, Y. J., Shea, P. J., Lee, W. H., Kim, H. M., & Oh, B. T. (2013). Removal of Pb(II) from aqueous solution by a zeolite–nanoscale zero-valent iron composite. *Chemical Engineering Journal, 217*, 54–60.

Klas, S., & Kirk, D. W. (2013). Advantages of low pH and limited oxygenation in arsenite removal from water by zero-valent iron. *Journal of Hazardous Materials, 252-253*, 77–82.

Kumar, N., Auffan, M., Gattacceca, J., Rose, J., Olivi, L., Borschneck, D., Kvapil, P., Jublot, M., Kaifas, D., Malleret, L., Doumenq, P., & Bottero, J. Y. (2014). Molecular insights of oxidation process of iron nanoparticles: spectroscopic, magnetic, and microscopic evidence. *Environmental Science & Technology, 48*(23), 13888–13894.

Li, X., & Shang, C. (2005). Role of humic acid and quinone model compounds in bromate reduction by zerovalent iron. *Environmental Science & Technology, 39*, 1092–1100.

Li, X. Q., Elliott, D. W., & Zhang, W. X. (2006). Zero-valent iron nanoparticles for abatement of environmental pollutants: materials and engineering aspects. *Critical Reviews in Solid State, 31*(4), 111–122.

Liao, C. H., Kang, S. F., & Hsu, Y. W. (2003). Zero-valent iron reduction of nitrate in the presence of ultraviolet light, organic matter and hydrogen peroxide. *Water Research, 37*(17), 4109–4118.

Liao, D. (2009). Kinetics of removing nitrate by nanoscale zero-valent iron. *Chinese Journal of Environmental Engineering*, 3(6): 985–989.

Liu, Y. C., Dionysios, H. C., & Lowry, G. V. (2005a). Trichloroethene hydro-dechlorination in water by highly disordered monometallic nanoiron. *Chemistry of Materials, 17*, 5315–5322.

Liu, Y. C., Majetich, S. A., Tilton, R. D. Sholl, D. S., Lowry, G. V.. (2005b). TCE dechlorination rates, pathways, and efficiency of nanoscale iron particles with different properties. *Environmental Science & Technology 39*(1338–1345).

Luo, S., Qin, P., Shao, J., Peng, L., Zeng, Q., & Gu, J. D. (2013). Synthesis of reactive nanoscale zero valent iron using rectorite supports and its application for Orange II removal. *Chemical Engineering Journal, 223*, 1–7.

Lv, X., Xu, J., Jiang, G., Tang, J., & Xu, X. (2012). Highly active nanoscale zero-valent iron (nZVI)-Fe3O4 nanocomposites for the removal of chromium(VI) from aqueous solutions. *Journal of Colloid and Interface Science, 369*(1), 460–469.

Manciulea, A., Baker, A., & Lead, J. R. (2009). A fluorescence quenching study of the interaction of Suwannee River fulvic acid with iron oxide nanoparticles. *Chemosphere, 76*(8), 1023–1027.

Neumann, A., Kaegi, R., Voegelin, A., Hussam, A., Munir, A. K., & Hug, S. J. (2013). Arsenic removal with composite iron matrix filters in Bangladesh: a field and laboratory study. *Environmental Science & Technology, 47*(9), 4544–4554.

Ryu, A., Jeong, S. W., Jang, A., & Choi, H. (2011). Reduction of highly concentrated nitrate using nanoscale zero-valent iron: effects of aggregation and catalyst on reactivity. *Applied Catalysis B: Environmental, 105*(1–2), 128–135.

Shi, J., Yi, S., He, H., Long, C., & Li, A. (2013). Preparation of nanoscale zero-valent iron supported on chelating resin with nitrogen donor atoms for simultaneous reduction of Pb^{2+} and NO_3^-. *Chemical Engineering Journal, 230*, 166–171.

Shimizu, A., Tokumura, M., Nakajima, K., & Kawase, Y. (2012). Phenol removal using zero-valent iron powder in the presence of dissolved oxygen: roles of decomposition by the Fenton reaction and adsorption/precipitation. *Journal of Hazardous Materials, 201-202*, 60–67.

Shuang, C., Wang, M., Zhou, Q., Zhou, W., & Li, A. (2013). Enhanced adsorption and antifouling performance of anion-exchange resin by the effect of incorporated Fe3O4 for removing humic acid. *Water Research, 47*(16), 6406–6414.

Sohn, K., Kang, S. W., Ahn, S., Woo, M., & Yang, S. K. (2006). Fe(0) nanoparticles for nitrate reduction: stability, reactivity, and transformation. *Environmental Science & Technology, 40*, 5514–5519.

Song, H., Yao, Z., Wang, M., Wang, J., Zhu, Z., & Li, A. (2013). Effect of dissolved organic matter on nitrate-nitrogen removal by anion exchange resin and kinetics studies. *Journal of Environmental Science China, 25*(1), 105–113.

Su, C., & Puls, R. W. (2004). Nitrate reduction by zerovalent iron: effects of formate, oxalate, citrate, chloride, sulfate, borate, and phosphate. *Environmental Science & Technology, 38*(9), 2715–2720.

Tombácz, E., Tóth, I. Y., Nesztor, D., Illés, E., Hajdú, A., Szekeres, M., et al. (2013). Adsorption of organic acids on magnetite nanoparticles, ph-dependent colloidal stability and salt tolerance. *Colloids Surfaces A, 435*(9), 91–96.

Vindedahl, A. M., Strehlau, J. H., Arnold, W. A., & Penn, R. L. (2016). Organic matter and iron oxide nanoparticles: aggregation, interactions, and reactivity. *Environmental Science: Nano, 3*(3), 494–505.

Xu, J., Hao, Z., Xie, C., Lv, X., Yang, Y., & Xu, X. (2012). Promotion effect of Fe^{2+} and Fe_3O_4 on nitrate reduction using zero-valent iron. *Desalination, 284*, 9–13.

Yang, K., Lin, D., & Xing, B. (2009). Interactions of humic acid with nanosized inorganic oxides. *Langmuir, 25*, 3571–3576.

Zhang, Y., Chen, Y., Westerhoff, P., Hristovski, K., & Crittenden, J. C. (2008). Stability of commercial metal oxide nanoparticles in water. *Water Research, 42*(8–9), 2204–2212.

Zhang, Q., Du, Q., Jiao, T., Pan, B., Zhang, Z., Sun, Q., et al. (2013a). Selective removal of phosphate in waters using a novel of cation adsorbent: zirconium phosphate (zrp) behavior and mechanism. *Chemical Engineering Journal, 221*(2), 315–321.

Zhang, Q., Du, Q., Hua, M., Jiao, T., Gao, F., & Pan, B. (2013b). Sorption enhancement of lead ions from water by surface charged polystyrene-supported nano-zirconium oxide composites. *Environmental Science & Technology, 47*(12), 6536–6544.

Zhang, Q., Li, Y., Phanlavong, P., Wang, Z., Jiao, T., Qiu, H., & Peng, Q. (2017). Highly efficient and rapid fluoride scavenger using an acid/base tolerant zirconium phosphate nanoflake: behavior and mechanism. *Journal of Cleaner Production, 161*, 317–326.

Zhang, Q., Li, Y., Yang, Q., Chen, H., Chen, X., Jiao, T., & Peng, Q. (2018). Distinguished Cr(VI) capture with rapid and superior capability using polydopamine microsphere: behavior and mechanism. *Journal of Hazardous Materials, 342*, 732–740.